J Mater Sci

Ceramics

$Li_5Ti_2O_6F$: a new low-loss oxyfluoride microwave dielectric ceramic for LTCC applications

Zhiwei Zhang[1], Ying Tang[1,2,*], Huaicheng Xiang[1], Aihong Yang[1], Yu Wang[1], Changzhi Yin[1], Yunfei Tian[1], and Liang Fang[1,3,*]

[1] *Guangxi Key Laboratory of Optical and Electronic Materials and Devices, College of Material Science and Engineering, Guilin University of Technology, Guilin 541004, People's Republic of China*

[2] *Key Laboratory of Nonferrous Materials and New Processing Technology, Ministry of Education, Guilin University of Technology, Guilin 541004, People's Republic of China*

[3] *College of Materials and Chemical Engineering, China Three Gorges University, Yichang 443002, People's Republic of China*

Received: 10 July 2019
Accepted: 11 September 2019

ABSTRACT

Use of microwave dielectric ceramics can significantly promote the development of communication devices. The primary criteria for determining their applications are excellent microwave dielectric properties and suitability for co-firing with cheap metals (e.g., Ag, Al). This study first reports the low-temperature synthesis of $Li_5Ti_2O_6F$ with a cubic rock salt structure. $Li_5Ti_2O_6F$ was prepared at 880 °C and had ε_r of 19.6, $Q \times f$ of 79500 GHz, and τ_f of − 29.6 ppm/ °C. The infrared reflectivity spectrum revealed that the dielectric contribution of $Li_5Ti_2O_6F$ in the microwave range was mainly affected by phonon absorption. Experimental study indicated that $Li_5Ti_2O_6F$ had good chemical compatibility versus Ag electrode at 880 °C for 2 h. Given these characteristics, $Li_5Ti_2O_6F$ ceramics exhibited potential for low-temperature co-fired ceramic technology.

Introduction

Low-temperature co-fired ceramic (LTCC) is an essential material for filters, oscillators, and antenna substrates, due to its fast transmission speed, powerful function, small size, and lightweight [1–6]. The requirements to obtain LTCCs with crucial performance are as follows: (1) optimal sintering temperature below the melting point of the inner metal electrode such as Ag (961 °C) and good chemical compatibility with the metal; (2) suitable range of relative permittivity (ε_r); (3) high quality factor ($Q \times f$); (4) close-to-zero temperature coefficient of resonant frequency (τ_f); (5) low cost of raw materials; and (6) low bulk density for lightness of the electronic devices [7–13].

Commercial microwave dielectric ceramics are made of high-temperature oxides, such as $CaTiO_3$, Al_2O_3, $Ba(Mg_{1/3}Ta_{2/3})O_3$, and $Ba(Zn_{1/3}Ta_{2/3})O_3$, which have sintering temperatures of about 1300 °C or even higher [14–17]. In addition, rock salt ceramics (Li_2TiO_3, $Li_2Mg_2TiO_5$, and $Li_2Mg_3SnO_6$) have good

Address correspondence to E-mail: tangyinggl001@aliyun.com; fanglianggl001@aliyun.com

https://doi.org/10.1007/s10853-019-04031-4

Published online: 01 October 2019

microwave dielectric properties and relatively high sintering temperatures (> 1200 °C) [18–20]. The most common method for decreasing the sintering temperature of ceramics is to add low-melting glasses, such as Li_2O–MgO–B_2O_3, B_2O_3–Bi_2O_3–SiO_2–ZnO, and $BaCu(B_2O_5)$ [21–24]. However, this process is accompanied by reduced microwave dielectric properties. In recent years, fluoride microwave dielectric ceramics with low sintering temperatures have attracted research attention. Lei et al. [25] reported various low-fired fluoride microwave dielectric ceramics (LiF, CaF_2, SrF_2, and BaF_2); in particular, LiF exhibits satisfactory performance (ε_r = 8.02, $Q \times f$ = 73880 GHz, τ_f = − 117.7 ppm/ °C) at 800 °C and thus could be used to develop LTCC. In this study, a new type of oxyfluoride ceramic, namely $Li_5Ti_2O_6F$, which possesses the advantages of low sintering temperature and high quality factor, was fabricated. The crystal structure, sintering characteristic, microwave dielectric properties, and chemical compatibility of $Li_5Ti_2O_6F$ with the Ag electrode were investigated.

Experimental procedure

Oxyfluoride $Li_5Ti_2O_6F$ samples were fabricated through a conventional solid-state reaction in the air by using high-purity raw materials including Li_2CO_3 (99.99%), TiO_2 (99.99%), and LiF (99.99%), which were weighed via the correct stoichiometry. The mixed powders were ball-milled in a nylon jar with ZrO_2 balls for 6 h by using ethanol as a medium at 180 rpm. The slurries were dried and calcined at 700 °C for 2 h. The calcined powders were re-milled for 6 h, dried, added with 5 wt% PVA as binder, and granulated. The resultant particles were pressed into cylinders with a diameter of 10 mm and a height of 6 mm and were heated to 550 °C for 4 h at a rate of 1.5 °C/min to remove the organic binder. Heating was continued up to 800 °C–900 °C for sintering. Powders of the same composition were covered in pellets and heated in an alumina crucible to limit Li evaporation during sintering. The chemical compatibility of $Li_5Ti_2O_6F$ and Ag was also investigated by co-firing the mixtures at 880 °C for 2 h.

The bulk densities of the sintered samples were measured by Archimedes method. Thermal behavior and phase evolution were evaluated using a NETZSCH STA449F3 thermogravimetric and differential scanning calorimetry analyzer (TG–DSC). The phase composition of $Li_5Ti_2O_6F$ was determined using an X-ray diffractometer ($CuK\alpha_1$, 1.54059 Å, model X'Pert PRO, PANalytical, Almelo, The Netherlands). The refinement XRD scan rate is 0.021154°/s. Energy-dispersive x-ray spectroscopy (EDS) and surface microstructures analyses of the specimens were performed using a field-emission scanning electron microscope (FE-SEM, model S4800, Hitachi, Japan). Selected area electron diffraction (SAED) patterns and high-resolution transmission electron microscope (HRTEM) images were collected by JEOL JEM-2100F TEM. The ε_r and $Q \times f$ of the sintered samples were measured in the TE_{011} mode according to the Hakki–Coleman method [26] using a network analyzer (model N5230A, Agilent Co., Palo Alto, CA). τ_f was measured using a temperature chamber (Delta 9039, Delta Design, San Diego, CA) and calculated using the following equation:

$$\tau_f = \frac{f_{85} - f_{25}}{(85 - 25) \times f_{25}} \times 10^6 \quad (1)$$

where f_{85} and f_{25} are the resonant frequencies at 85 °C and 25 °C, respectively.

Room-temperature infrared reflectivity spectra were recorded using a Bruker IFS 66v FTIR spectrometer on infrared beamline station (U4) at National Synchrotron Radiation Lab (NSRL), Hefei, China. The infrared reflectivity spectra were analyzed by the harmonic oscillator model (the Lorentz three-parameter classical model) as follows: [27, 37]

$$\varepsilon^*(\omega) = \varepsilon_\infty + \sum_{j=1}^{n} \frac{\omega_{pj}^2}{\omega_{oj}^2 - \omega^2 - j\omega\gamma_j} \quad (2)$$

where $\varepsilon^*(\omega)$ is the complex dielectric function, ε_∞ is the dielectric constant caused by the electronic polarization at high frequencies, γ_j, ω_{oj}, and ω_{pj} are the damping factor, the transverse frequency, and plasma frequency of the jth Lorenz oscillator, respectively, and n is the number of transverse phonon modes. The complex reflectivity $R(\omega)$ can be written as:

$$R(\omega) = \left| \frac{1 - \sqrt{\varepsilon*(\omega)}}{1 + \sqrt{\varepsilon*(\omega)}} \right|^2 \quad (3)$$

Results and discussion

Figure 1 presents the room-temperature XRD patterns of $Li_5Ti_2O_6F$ powders calcined at various temperatures for 2 h. The diffraction peak was indexed to the monoclinic Li_2TiO_3 phase (JCPDS#330831) with the C2/c space group when calcined at 750 °C. The intensity of the (002) supercell diffraction peak decreased with increasing calcination temperature and basically disappeared when calcined at 800 °C. Hence, phase evolution occurred from order monoclinic to disorder cubic structure. This phenomenon confirmed with the results of the TG–DSC analysis (Fig. 2). At temperatures above 800 °C, the peaks were consistent with the cubic Li_2TiO_3 phase (JCPDS#031024, Fm-3m space group). No trace of an impurity phase was detected.

Figure 2 shows the TG–DSC curves of the dried mixed raw material powders from 30 to 900 °C. In the DSC curve, an endothermic peak existed between 500 and 650 °C, corresponding to a mass loss of about 27% on the TG curve due to the thermal decomposition of Li_2CO_3. According to the phase diagram of Li_2CO_3–LiF [28], when Li_2CO_3 and LiF were mixed in 2:1 mol ratio, Li_2CO_3 was decomposed at 630 °C, consistent with our test result (625 °C). The exothermic peak at 800 °C was attributed to the phase transition of the monoclinic to the cubic structure and was verified from the XRD patterns.

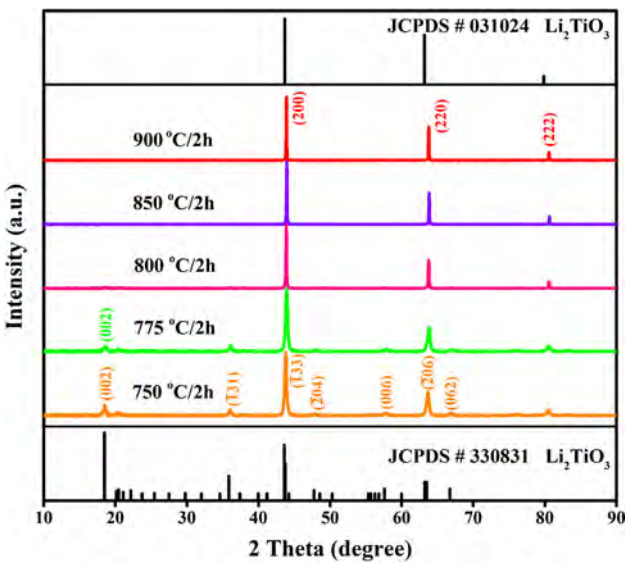

Figure 1 XRD patterns of $Li_5Ti_2O_6F$ powders calcined at various temperatures.

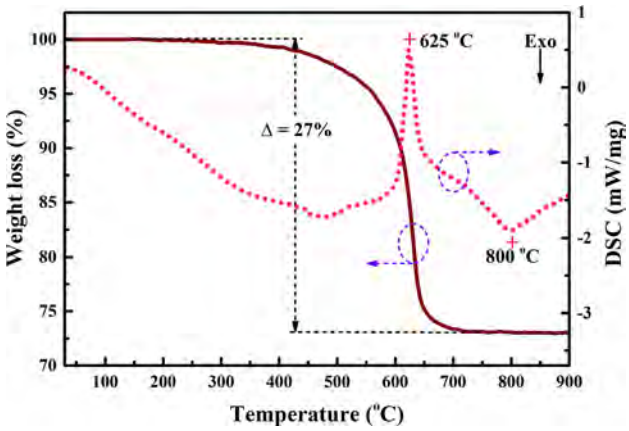

Figure 2 TG–DSC curves of $Li_5Ti_2O_6F$ powders from 30 to 900 °C.

Rietveld refinement of XRD was carried out using FullProf software to study the crystal structure of $Li_5Ti_2O_6F$, as shown in Fig. 3a. The refinement confirmed that $Li_5Ti_2O_6F$ had a cubic structure with a space group Fm-3m. The results of the refined parameters were $a = b = c = 4.1325(1)$ Å, $\alpha = \beta = \gamma = 90°$, and $V_m = 70.5730(5)$ Å^3, whereas the refinement reliability factors R_p, R_{wp}, and R_{exp} were 4.78%, 8.44%, and 6.2%, respectively, indicating a reliable result. The schematic of the crystal structure of rock-salt-type $Li_5Ti_2O_6F$ is illustrated in Fig. 3a. The O/F anions randomly stacking in a cubic close packing with Li/Ti cations occupied the octahedron sites. SAED patterns and the corresponding HRTEM images were recorded along the [111] zone axis to further verify the structure of $Li_5Ti_2O_6F$ ceramic (Fig. 3b, c). The lattice fringes of the sample were 0.15 and 0.15 nm for the $d_{(02\bar{2})}$ and $d_{(20\bar{2})}$ spacing, respectively, which corresponded with the cubic rock salt structure.

Figure 4a–f shows the surface microstructures of $Li_5Ti_2O_6F$ ceramics sintered at various temperatures. The grain size increased, whereas the size of pores decreased with increasing temperature. Moreover, a dense and homogeneous microstructure was obtained in the samples sintered at 880 °C (Fig. 4e). The grain size distributions and the average grain size of $Li_5Ti_2O_6F$ are given in the inset of Fig. 4a–f. The average grain size increased from 6.75 to 14.79 μm when the temperature increased from 800 to 880 °C. However, abnormally large grains and a small number of pores were observed in the sample sintered at 900 °C. Element mapping of the samples sintered at 880 °C was conducted to confirm the

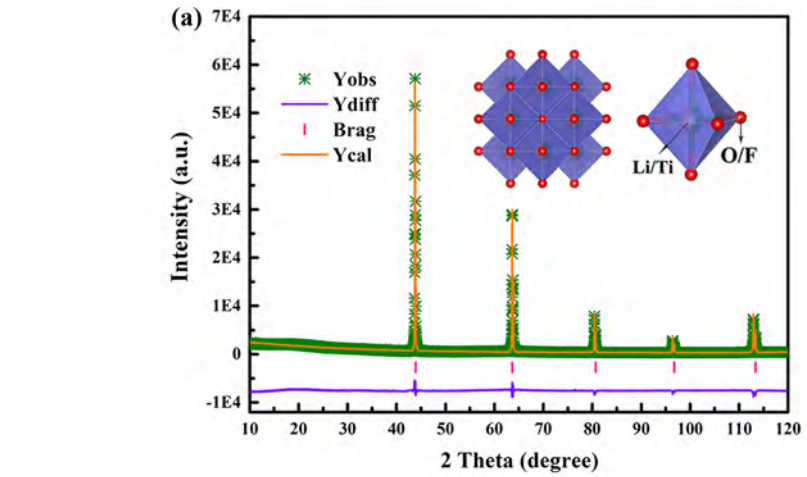

Figure 3 **a** Rietveld refinement of samples sintered at 880 °C and schematic of the crystal structure for $Li_5Ti_2O_6F$. **b** SAED pattern of $Li_5Ti_2O_6F$ sample sintered at 880 °C. **c** HRTEM images of $Li_5Ti_2O_6F$ ceramic recorded along the [111] zone axis.

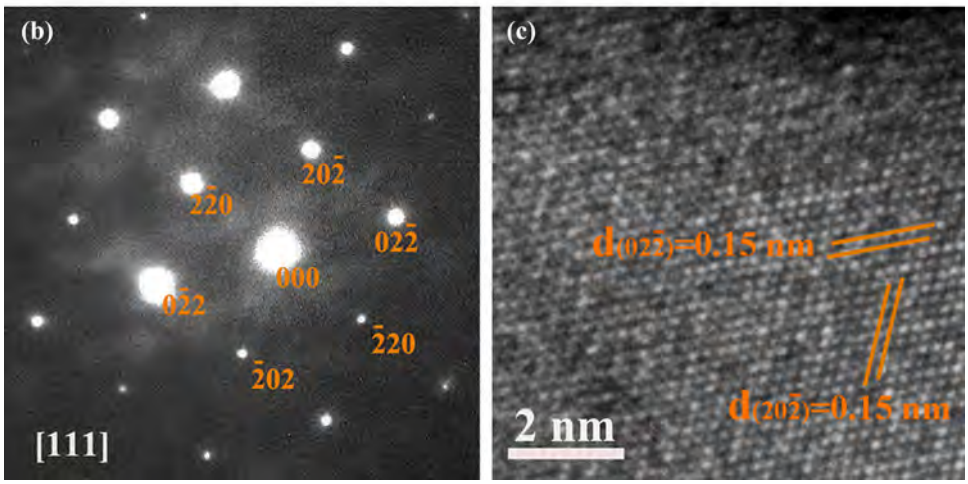

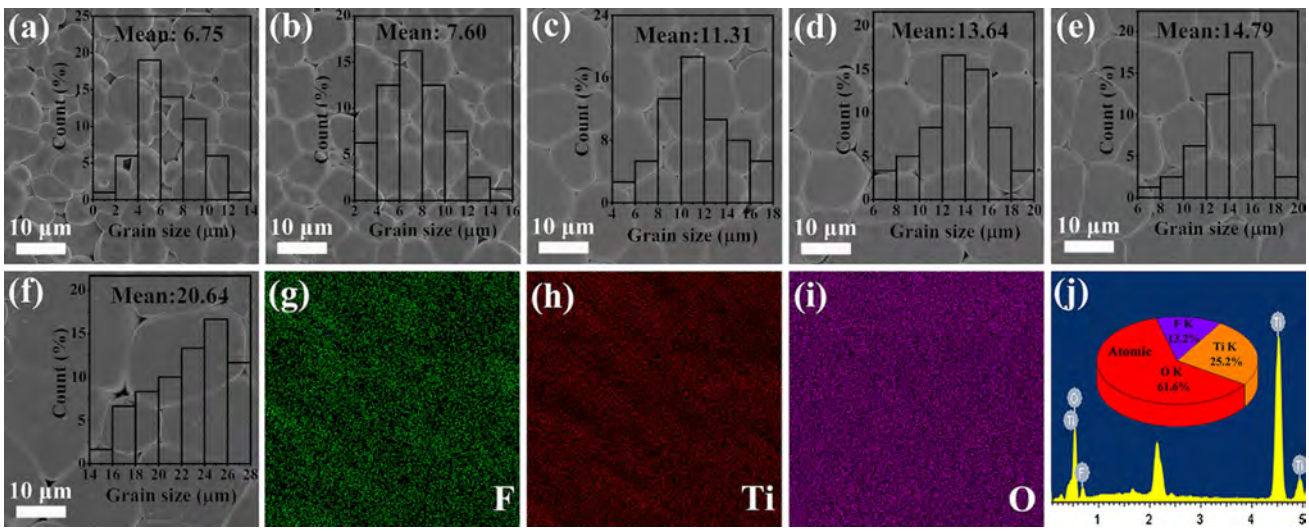

Figure 4 FE-SEM images of the surfaces of the sintered ceramic at: **a** 800 °C, **b** 820 °C, **c** 840 °C, **d** 860 °C, **e** 880 °C, and **f** 900 °C for $Li_5Ti_2O_6F$ and corresponding EDS analysis surface scanning of **g** F, **h** Ti, **i** O, **j** EDS spectrum.

element distribution (Fig. 4g–i). All the elements, namely F, Ti, and O, were distributed homogeneously. Element enrichment was not observed at the grain boundary, indicating that LiF

with Li_2TiO_3 completely formed a solid solution. In addition, EDS analysis of the surface of the $Li_5Ti_2O_6F$ ceramics sintered at 880 °C was also performed (Fig. 4j). The energy spectrum confirmed the existence of Ti, O, and F, and the ratio of each element was relatively close to the nominal composition.

The variations in the bulk density and relative density of the $Li_5Ti_2O_6F$ ceramic sintered at 800 °C–900 °C are depicted in Fig. 5a. With increasing sintering temperature, the bulk density gradually increased and reached the saturated value of 3.12 g/cm^3 at 880 °C. The relative density of 94% slightly decreased with increasing sintering temperature. Figure 5b presents the ε_r of $Li_5Ti_2O_6F$ ceramic as a function of sintering temperature. The variation tendency of ε_r was similar to that of relative density, that is, the influence of porosity on ε_r plays an important role. ε_r can then be corrected by the Bosman–Havinga formula [29]:

$$\varepsilon_{corr} = \varepsilon_r(1 + 1.5P) \tag{4}$$

$$P = 1 - \frac{\rho_{mea}}{\rho_{th}} \tag{5}$$

where P denotes the fractional porosity; ρ_{mea} and ρ_{th} are the measured and theoretical values of density, respectively. The corrected permittivity (ε_{corr}) values (Fig. 5b) fluctuate at around 21, which was higher than the measured value (18.1–19.6) of the samples sintered at 800 °C–900 °C. Furthermore, the theoretical permittivity (ε_{th}) can be computed using total ionic polarizability of individual ions and the molar volume of a compound in accordance with the Clausius–Mossotti equation: [30]

$$\varepsilon_{th} = \frac{3V_m + 8\pi\alpha_D^T}{3V_m - 4\pi\alpha_D^T} \tag{6}$$

where V_m and α_D^T represent cell volume and molecular polarizability, respectively. The sum of ionic polarizability of $Li_5Ti_2O_6F$ can be calculated with the additive rule:

$$\alpha\left(Li_{\frac{5}{7}}Ti_{\frac{2}{7}}O_{\frac{6}{7}}F_{\frac{1}{7}}\right) = \frac{5}{7}\alpha(Li^+) + \frac{2}{7}\alpha(Ti^{4+}) + \frac{6}{7}\alpha(O^{2-}) + \frac{1}{7}\alpha(F^-) \tag{7}$$

where $\alpha(Li^+)$, $\alpha(Ti^{4+})$, $\alpha(O^{2-})$, and $\alpha(F^-)$ are 1.2, 2.93, 2.01, and 1.62 A^3, respectively [29, 31]. According to Eq. (6), $Li_5Ti_2O_6F$ ceramic has a theoretical permittivity of 20.7, which is comparable to the measured value.

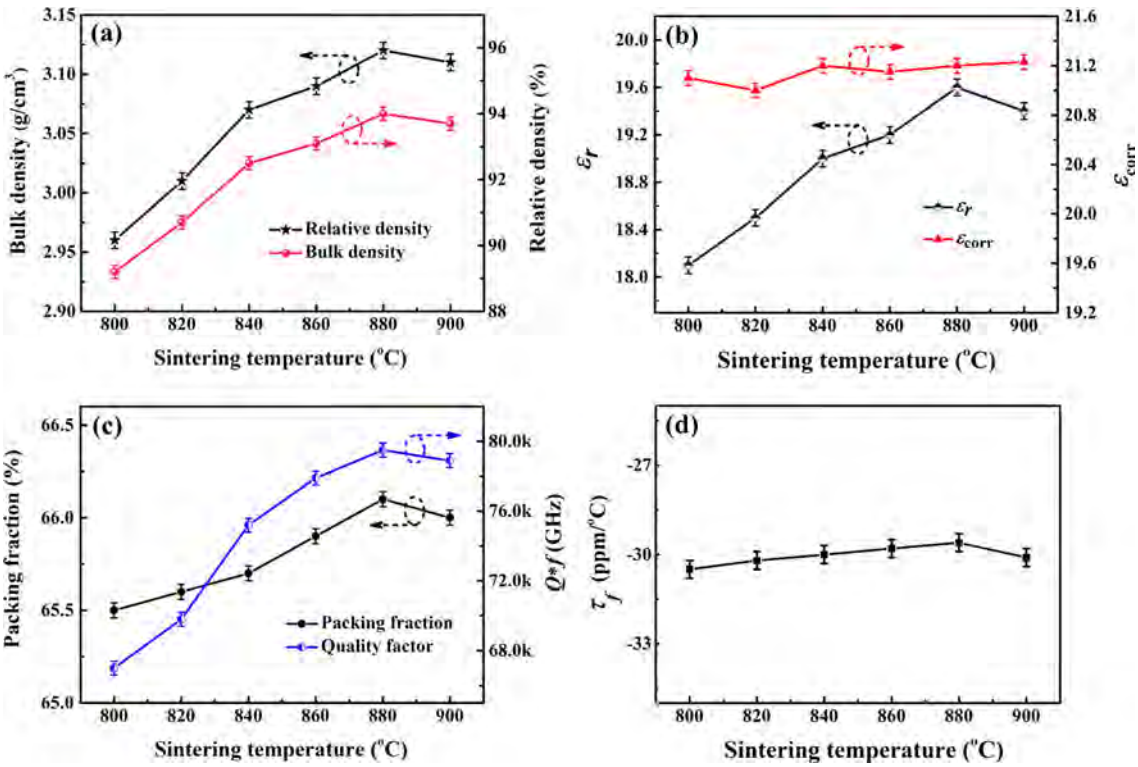

Figure 5 **a** Bulk density and relative density, **b** relative permittivity (ε_r and ε_{corr}), **c** packing fraction and quality factor ($Q \times f$), and **d** temperature coefficient of resonance frequency (τ_f) of $Li_5Ti_2O_6F$ ceramics sintered at 800–900 °C for 2 h.

The $Q \times f$ values of $Li_5Ti_2O_6F$ ceramic increased from 67000 to 79500 GHz as the sintering temperature was increased from 800 to 880 °C (Fig. 5c). In general, $Q \times f$ value was influenced by external factors, such as density, impurity, and secondary phase, and internal factors, such as crystal structure [32, 33]. Packing fraction theory was proposed to explain the quality factor and defined as Eq. (8) [34]:

$$\text{packing fraction}(\%) = \frac{\text{volume of packed ions}}{\text{volume of unit cell}} \times Z = \frac{\left(\frac{4\pi}{3}\right)\left(r_{Li}^3 + r_{Ti}^3 + r_O^3 + r_F^3\right)}{V} \times 4 \quad (8)$$

The packing fraction was positively correlated with $Q \times f$, as shown in Fig. 5c. An increase in the packing fraction reduced the vibration of the crystal lattice, causing an increase in the quality factor [35]. The maximum calculated packing fraction was 66.1% when $Li_5Ti_2O_6F$ ceramic was sintered at 880 °C. As shown in Fig. 5d, the τ_f values of $Li_5Ti_2O_6F$ ceramic were not temperature dependent and remained stable at around − 30 ppm/ °C. In summary, $Li_5Ti_2O_6F$ ceramic sintered at 880 °C exhibited the optimum microwave dielectric properties with ε_r = 19.6, $Q \times f$ = 79500 GHz, and τ_f = − 29.6 ppm/°C.

Infrared reflectivity spectrum was used to investigate inherent dielectric properties [36, 37]. Figure 6 shows the IR reflectivity spectrum of $Li_5Ti_2O_6F$ ceramic sintered at 880 °C. The fitting of reflectivity spectrum was performed by REFFIT software, and processing procedure is similar as described in our previous work [12, 36]. As listed in Table 1, the relative permittivity at high frequencies (ε_∞) was 5.71, and the intrinsic permittivity ε_0 (extrapolated value) was 19.4, which was close to the measured value of 19.6. The permittivity of $Li_5Ti_2O_6F$ ceramic was mainly attributed to the dielectric response of intrinsic phonons. Furthermore, dielectric loss can be calculated by the following formula:

$$\varepsilon' = \varepsilon_\infty + \sum_{j=1}^{n} \frac{\omega_{pj}^2}{\omega_{oj}^2} = \varepsilon_\infty + \sum_{j=1}^{n} \Delta\varepsilon_j \quad (9)$$

$$\tan\delta = \frac{\varepsilon''}{\varepsilon'} = \omega \sum_{j=1}^{n} \frac{\Delta\varepsilon_j \gamma_j}{\omega_{oj}^2\left(\varepsilon_\infty + \sum_{j=1}^{n} \Delta\varepsilon_j\right)} \quad (10)$$

The calculated dielectric loss was 9.8×10^{-5} (f = 9.5 GHz, $Q = 1/\tan\ \delta$, $Q \times f$ = 97000 GHz), which was lower than the measured value of 1.2×10^{-4} ($Q \times f$ = 79500 GHz). The deviation between the calculated and measured quality factor might be attributed to extrinsic factors, such as pores and uneven distribution of grain size of the sintered sample. Therefore, quality factor can be improved by reducing the porosity and optimizing the preparation process.

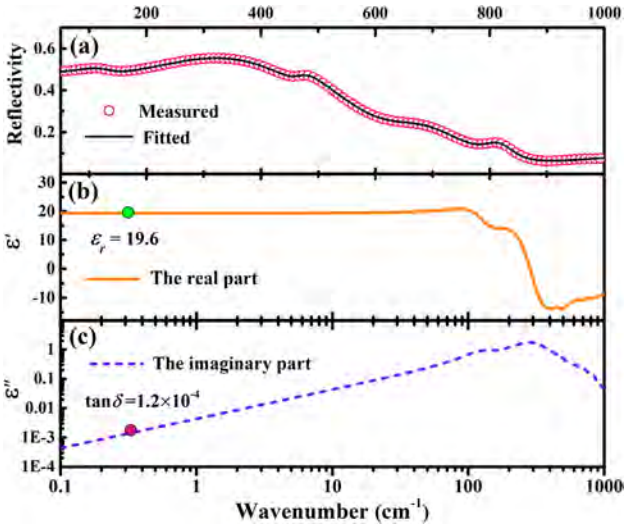

Figure 6 **a** Measured and fitted IR reflectivity spectra of the $Li_5Ti_2O_6F$ ceramic within 50–1000 cm^{-1}. **b** The yellow solid line is the real part. **c** The purple dotted line is the imaginary part.

Table 1 Phonon parameters obtained by fitting of the infrared reflectivity spectrum of $Li_5Ti_2O_6F$ ceramic

Mode	ω_{oj}	ω_{pj}	γ_j	$\triangle\varepsilon_j$
1	128.18	252.8	75.605	1.6740
2	306.58	1376.6	234.66	17.200
3	470.29	215.3	55.175	0.2100
4	489.7	323.22	276.43	0.4360
5	677.58	501.51	194.50	0.5480
6	812.56	226.45	63.506	0.0747
	$Li_5Ti_2O_6F$ ε_∞ = 5.71 ε_0 = 19.4			

$Li_5Ti_2O_6F$ powders were co-fired with Ag powders to study the chemical compatibility of ceramics with metal electrodes. Figure 7 shows the XRD pattern, EDS, and BSEM images of pure $Li_5Ti_2O_6F$ and $Li_5Ti_2O_6F$ co-fired with 20 wt% Ag powders sintered at 880 °C for 2 h. The peaks of $Li_5Ti_2O_6F$ and Ag phases were observed, indicating their good chemical compatibility. Two kinds of grains with different sizes and shapes were detected in the BSE image. The brighter grains marked with "spot" were identified

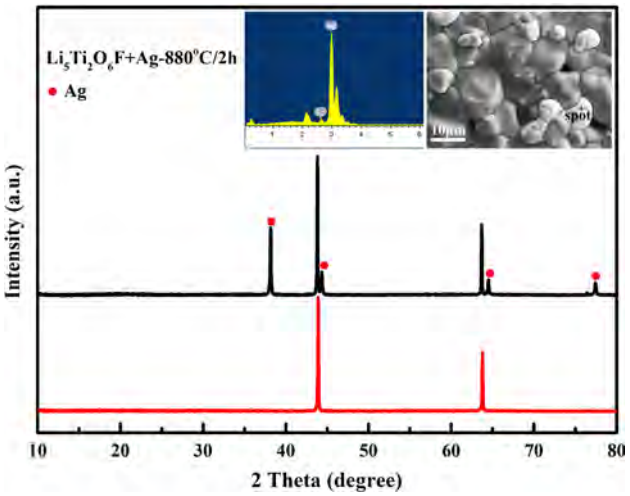

Figure 7 XRD and BSEM analyses of $Li_5Ti_2O_6F$ ceramic co-fired with 20 wt% Ag at 880 °C for 2 h.

through elemental analysis with EDS as Ag. All the results indicated the lack of chemical reaction between $Li_5Ti_2O_6F$ and Ag; as such, $Li_5Ti_2O_6F$ exhibits potential for application in LTCC technology.

Conclusions

In this work, a new oxyfluoride, $Li_5Ti_2O_6F$, was synthesized using traditional solid-state reaction method at 800 °C. The XRD Rietveld refinement revealed that $Li_5Ti_2O_6F$ belongs to a cubic structure with a space group Fm-3m. The SAED patterns and corresponding HRTEM images confirmed the structure. After sintering at 880 °C, $Li_5Ti_2O_6F$ ceramic exhibited the optimum microwave dielectric properties: $\varepsilon_r = 19.6$, $Q \times f = 79500$ GHz, and $\tau_f = -29.6$ ppm/ °C. The results of the far-infrared reflectivity test revealed that the polarization of the $Li_5Ti_2O_6F$ ceramic in the microwave region was mainly attributed to the absorption of phonon oscillation in the infrared region and that the defect phonon scattering had minimal effect. Moreover, $Li_5Ti_2O_6F$ ceramic was found to be chemically compatible with Ag. Hence, $Li_5Ti_2O_6F$ ceramic is a potential candidate for LTCC applications.

Acknowledgements

We appreciate the administrators of the IR beamline workstation of the National Synchrotron Radiation Laboratory (NSRL) for their help in IR measurements. This work was supported by the Natural Science Foundation of China (Nos. 21561008, 21965009), the Natural Science Foundation of Guangxi Zhuang Autonomous Region (Nos. 2015GXNSFFA139003, 2018GXNSFAA138175), Project of Scientific Research and Technical Exploitation Program of the Guangxi Zhuang Autonomous Region (Nos. AA18118008, AA18118034, AA18118023) and Guilin (20170225), and Innovation Project of Guangxi Graduate Education (YCSW2019157).

References

[1] Sebastian MT, Jantunen H (2008) Low loss dielectric materials for LTCC applications: a review. Int Mater Rev 53:57–90

[2] Seo YJ, Shin DJ, Cho YS (2006) Phase evolution and microwave dielectric properties of lanthanum borate-based low-temperature co-fired ceramics materials. J Am Ceram Soc 89:2352–2355

[3] Sebastian MT, Wang H, Jantunen H (2016) Low temperature co-fired ceramics with ultra-low sintering temperature: a review. Curr Opin Solid State Mater Sci 20:151–170

[4] Joseph N, Varghese J, Siponkoski T, Teirikangas M, Sebastian MT, Jantunen H (2016) Glass-free CuMoO4 ceramic with excellent dielectric and thermal properties for ultralow temperature cofired ceramic applications. ACS Sustain Chem Eng 4:5632–5639

[5] Ohsato H (2012) Functional advances of microwave dielectric for next generation. Ceram Int 38:S141–S146

[6] Cava RJ (2001) Dielectric materials for applications in microwave communications. J Mater Chem 11:54–62. https://doi.org/10.1039/B003681L

[7] Xia C-C, Jiang D-H, Chen G-H (2017) Microwave dielectric ceramic of $LiZnPO_4$ for LTCC applications. J Mater Sci: Mater Electron 28:12026–12031

[8] Zhou D, Guo D, Li W-B, Pang L-X, Yao X, Wang D-W, Reaney IM (2016) Novel temperature stable high-ε_r microwave dielectrics in the Bi_2O_3–TiO_2–V_2O_5 system. J Mater Chem C 4:5357–5362. https://doi.org/10.1039/C6TC01431C

[9] Zhou D, Pang L-X, Wang D-W, Li C, Jin B-B, Reaney IM (2017) High permittivity and low loss microwave dielectrics suitable for 5G resonators and low temperature co-fired ceramic architecture. J Mater Chem C 5:10094–10098. https://doi.org/10.1039/C7TC03623J

[10] Zhou D, Pang L-X, Wang D-W, Reaney IM (2018) BiVO4 based high k microwave dielectric materials: a review. J Mater Chem C 6:9290–9313. https://doi.org/10.1039/C8TC02260G

[11] Pang L-X, Zhou D (2019) Modification of NdNbO4 microwave dielectric ceramic by Bi substitutions. J Am Ceram Soc 102:2278–2282

[12] Chen J-Q, Tang Y, Xiang H-C, Fang L, Porwal H, Li C-C (2018) Microwave dielectric properties and infrared reflectivity spectra analysis of two novel low-firing AgCa2B2V3O12 (B = Mg, Zn) ceramics with garnet structure. J Eur Ceram Soc 38:4670–4676

[13] Wang R, Zhou J, Li B, Li L-T (2009) CaF2–AlF3–SiO2 glass-ceramic with low dielectric constant for LTCC application. J Alloys Compds 490:204–207

[14] Dou ZM, Jiang J, Wang G, Zhang F, Zhang T-J (2016) Effect of Ga^{3+} substitution on the microwave dielectric properties of $0.67CaTiO_3$–$0.33LaAlO_3$ ceramics. Ceram Int 42:6743–6748

[15] Alford NM, Penn SJ (1996) Sintered alumina with low dielectric loss. J Appl Phys 80:5895–5898

[16] Tolmer V, Desgardin G (1997) Low-temperature sintering and influence of the process on the dielectric properties of $Ba(Zn_{1/3}Ta_{2/3})O_3$. J Am Ceram Soc 80:1981–1991

[17] Ichinose N, Shimada T (2006) Effect of grain size and secondary phase on microwave dielectric properties of Ba(Mg1/3Ta2/3)O3 and Ba([Mg, Zn]1/3Ta2/3)O3 systems. J Eur Ceram Soc 26:1755–1759

[18] Yuan L-L, Bian J-J (2009) Microwave dielectric properties of lithium contained ceramics with rock salt structure. Ferroelectrics 387:123–129

[19] Li C-C, Xiang H-C, Yin C-Z, Tang Y, Li Y-C, Fang L (2018) Ultra-low loss microwave dielectric ceramic $Li_2Mg_2TiO_5$ and low-temperature firing Via B_2O_3 addition. J Electron Mater 47:6383–6389

[20] Fu Z-F, Liu P, Ma J-L, Zhao X-G, Zhang H-W (2016) Novel series of ultra-low loss microwave dielectric ceramics: $Li_2Mg_3BO_6$ (B = Ti, Sn, Zr). J Eur Ceram Soc 36:625–629

[21] Chen G-H, Hou M-Z, Yun Y (2012) Microwave dielectric properties of low-fired Li_2TiO_3 ceramics doped with Li_2O–MgO–B_2O_3 frit. Mater Lett 89:16–18

[22] Liu C, Zhang H-W et al (2015) Low temperature sintering BBSZ glass modified $Li_2MgTi_3O_8$ microwave dielectric ceramics. J Alloys Compd 646:1139–1142

[23] Xiao M, Gu Q-Q, Zhou Z-Q, Zhang P (2018) Low temperature sintering behavior and microwave dielectric properties of $LaNbO_4$ ceramics with $BaCu(B_2O_5)$ additive. J Alloys Compd 730:528–532

[24] Liang J, Lu W-Z (2009) Microwave dielectric properties of Li_2TiO_3 ceramics doped with ZnO–B_2O_3 frit. J Am Ceram Soc 92:952–954

[25] Song X-Q, Du K, Lei W et al (2019) Low-fired fluoride microwave dielectric ceramics with low dielectric loss. Ceram Int 45:279–286

[26] Hakki BW, Coleman PD (1960) A dielectric resonant method of measuring inductive capacitance in the millimeter range. IRE Trans Microwave Theory Technol 8:402–410

[27] Chen Z, Jia H, Sharafudeen K, Dai W-B, Liu Y-B, Dong G-Q, Qiu J-R (2016) Up-conversion luminescence from single vanadate through blackbody radiation harvesting broadband near-infrared photons for photovoltaic cells. J Alloys Compd 663:204–210

[28] Sangster J, Pelton AD (1987) Phase diagrams and thermodynamic properties of the 70 binary alkali halide systems having common ions. J Phys Chem Refer Data 16:509–561

[29] Bosman AJ, Havinga EE (1963) Temperature dependence of dielectric constants of cubic ionic compounds. Phys Rev 129:1593–1600

[30] Shannon RD (1993) Dielectric polarizabilities of ions in oxides and fluorides. J Appl Phys 73:348–366

[31] Park HS, Yoon KH, Kim ES (2001) Relationship between the bond valence and the temperature coefficient of the resonant frequency in the complex perovskite $(Pb_{1-x}Ca_x)[Fe_{0.5}(Nb_{1-y}Ta_y)_{0.5}]O_3$. J Am Ceram Soc 84:99–103

[32] Li C-C, Xiang H-C, Fang L et al (2018) Low-firing and temperature stable microwave dielectric ceramics $Ba_2LnV_3O_{11}$ (Ln = Nd, Sm). J Am Ceram Soc 101:773–781

[33] Li C-C, Xiang H-C, Xu M-Y, Tang Y, Fang L (2018) Li2AGeO4 (A = Zn, Mg): two novel low-permittivity microwave dielectric ceramics with olivine structure. J Eur Ceram Soc 38:1524–1528

[34] Kim ES, Chun BS, Freer RF, Cerni RJ (2010) Effects of packing fraction and bond valence on microwave dielectric properties of $A^{2+}B^{6+}O_4$(A^{2+}:Ca, Pb, Ba; B^{6+}: Mo, W) ceramics. J Eur Ceram Soc 30:1731–1736

[35] Xiang H-C, Li C-C, Jantunen H, Fang L, Hill AE (2018) Ultralow loss $CaMgGeO_4$ microwave dielectric ceramic and its chemical compatibility with silver electrodes for low-temperature cofired ceramic applications. ACS Sustain Chem Eng 6:6458–6466

[36] Zhang Z-W, Fang L, Xiang H-C, Li CC et al (2019) Structural, infrared reflectivity spectra and microwave dielectric properties of the $Li_7Ti_3O_9F$ ceramic. Ceram Int 45:10163–10169

[37] Guo J, Zhou D, Wang L, Wang H, Shao T, Qi Z-M, Yao X (2013) Infrared spectra, Raman spectra, microwave dielectric properties and simulation for effective permittivity of

temperature stable ceramics $AMoO_4$–TiO_2 (A = Ca, Sr). Dalton Trans 42:1483–1491